J Supercond Nov Magn (2016) 29:3147–3154
DOI 10.1007/s10948-016-3626-8

ORIGINAL PAPER

# Comparative Study of the Magnetic Structure of $BaFe_2As_2$ Doped with Co or Ni

**Jacques Soullard**[1] · **Ilya G. Kaplan**[2]

Received: 11 May 2016 / Accepted: 11 July 2016 / Published online: 16 August 2016
© Springer Science+Business Media New York 2016

**Abstract** We present a comparative study of the electronic structure of pure, Co-doped, and Ni-doped $BaFe_2As_2$. The calculations were performed by the embedded cluster method at the electron correlation level (ECM-MP2). The orbital population analysis reveals that doping with Co or Ni introduces, in both cases, a considerable transfer of charge from cations toward the anions and a transfer of spin density in the opposite direction that reflects an independence of spin and charge in non-relativistic approach. In both doping, we note the presence of spinless electron on the 3d orbitals. On the other hand, both doping cases differ in the local magnetic order: Co induces a local antiferromagnetic order along the b axis of the crystalline structure, while Ni maintains the ferromagnetic order along this axis. In the Co-doped compound, the frustration of magnetic state and formation of spinless electrons correspond to some properties of the Anderson RVB model of superconductivity.

**Keywords** Doped pnictide · Superconductivity · Ferromagnetism · Antiferromagnetism

✉ Jacques Soullard
soullard@fisica.unam.mx

Ilya G. Kaplan
kaplan@unam.mx

[1] Instituto de Física, UNAM, Apartado Postal 20-364, 01000 Ciudad de México, México

[2] Instituto de Investigación Materiales, UNAM, Apartado Postal 70-360, 04510 Ciudad de México, México

## 1 Introduction

Iron pnictides are the new family of high critical temperature superconductors recently discovered [1, 2]. They can be classified on six groups of iron-based compounds presenting superconductivity with a high critical temperature, see review [3]. The most studied of these groups is the 122 system such as $AFe_2As_2$ (with A = Ca, Sr, Ba, or Eu). The superconductivity (SC) appears under hole doping in the plane of A atoms (e.g., Ba substitution by K) or under electron doping (e.g., Fe substitution by Co or Ni) and in some other substitutions, see below.

In experiments, the Ba-based 122 system has been widely used for the availability of large and high-quality single crystals and for the possibility to produce SC materials on a variety of chemical doping. At room temperature, the undoped material, $BaFe_2As_2$, is a paramagnetic semimetal that undergoes structural and magnetic transitions at 140 K [4]. The tetragonal-to-orthorhombic transition is associated with the onset of antiferromagnetic (AFM) order [5, 6].

In 122-type materials, SC was first detected by Co substitution of Fe in $SrFe_2As_2$ [7] and $BaFe_2As_2$ [8]. It is induced also by several types of d-metal substitution. This includes the use of any elements in the Fe, Co, and Ni columns in the Periodical Table (except, so far, Os), see ref. [9] and references therein; but it excludes Cr [10], Mo [11], Mn [12], and Cu [13, 14]. At present, it is not clear why Co and Ni located on the electron-doping side of Fe produce a SC state, while Mn, Cr, and Mo located on the hole-doping side do not. It should be mentioned that the isovalent doping (e.g., substitution of Fe by Ru [15]) also gives rise to superconductivity. In this case, one should take into account a distinction between charge doping and chemical substitution.

Just after the discovery of the Fe SC, the density functional theory (DFT) calculations revealed main features of the electronic structure of doped and undoped $BaFe_2As_2$ compounds. It was shown that they have a quite complicated band structure and several disconnected Fermi surfaces (FSs) [16, 17]. All five 3d orbitals of Fe are involved in the electronic structure of FSs. There are two types of FSs: three hole FSs are located in the center of the Brillouin zone, and two electron FSs are located at the corner.

Very soon, it was accepted that the Fe superconductors possess nonconventional SC with an electron-pairing mechanism that has not been observed before [17–20]. Calculations of magnetic susceptibility [17] showed that these new superconducting materials have a tendency to form AFM order, and the magnetism existing in the parent crystal at zero doping is suppressed by the AFM spin fluctuations; it is also demonstrated that the wave vectors associated with the spatial periodicity of the magnetic moments coincide with those connecting the centers of the electron and hole FSs. Based on this, Mazin et al. [17] proposed that AF spin fluctuations can induce $s$-wave pairing with sign reversal of the order parameter between electron- and hole-like FSs; this kind of pairing is denoted as $s_{\pm}$. The latter was obtained also in ref. [21], while the authors [21] did not exclude the $d$-wave pairing as a possible candidate; see also the recent arguments against the $s_{\pm}$ pairing [22].

In many theoretical studies [23–25], the Fe superconductors are considered as doped Mott insulators with effective nearest-neighbor (nn) and next-nearest-neighbor (nnn) antiferromagnetic exchange interaction. In this model, antiferromagnetism [23, 24] and $s_{\pm}$ pairing [24, 25] are also revealed. It should be mentioned that, as discussed in review [26], the Anderson resonating valence bond (RVB) state of high-$T_c$ SC can be naturally applied in the Mott insulator model.

Anderson [27] proposed his RVB model for high-temperature superconductors just after the discovery of high-$T_c$ copper superconductors. According to Anderson, in the RVB state the antiferromagnetic (Néel) lattice will be melted into a spin-liquid phase consisting of singlet pairs. Upon carrier doping, these singlets would become charged, resulting in the SC state. Basing on the so-called separation of charge and spin, the electronic excitation spectra in the RVB state can be presented as two separated branches: charge spinless holons and chargeless spinons [28, 29]; see also the discussion between Anderson and Schrieffer in ref. [30].

Recently, Anderson's RVB ideas were applied by Poilblanc et al. [31] to construct a family of fermionic projected entangled pair states on a square lattice. They showed that under doping, the insulating RVB spin liquid evolves into a superconducting state with mixed $d + \imath s$ pairing symmetry, where the relative weight between $s$ and $d$ components is controlled by a variational parameter $c$. Optimizing the hole kinetic energy with respect to $c$, authors [31] obtained a sufficiently good description of the frustrated spin-1/2 $J_1$-$J_2$ AFM Heisenberg model proposed earlier for iron pnictide superconductors [32, 33]. The orbital symmetry of the optimized RVB superconductor has predominant d-wave character.

The iron pnictides belong to the broad category of strongly correlated superconductors, such as heavy fermions or cuprate high-temperature superconductors, which cannot be described in terms of weakly interacting quasiparticles. Usually, the strong electron correlation in solids is associated with the proximity of the Mott-insulating state. Last years, the role of Hund's intra-atomic exchange in creating strong correlation in materials that are not close to Mott's insulator was intensively discussed [34–37]. This allows to introduce the term *Hund's metals* [35]. The detailed physical description of Hund's metals is presented in review [37].

The theory of Hund's metals gives relevant information on the properties of doped iron-based compounds in the case of strong Hund's coupling [38]. For instance, an antiferromagnetic (AFM) order is predicted in the electron-doped regime; this is the case of Co-doped $BaFe_2As_2$ where AFM order has been revealed by neutron and X-rays studies [39]. The strong electron correlation is also responsible for magnetism in iron pnictide superconductors. In the case of Ni-doped $BaFe_2As_2$, inelastic neutron scattering allowed to determine the size of the fluctuating magnetic moment on Ni, $< m^2 >= 3.2(\mu_B)^2$ [40].

In this paper, we present a comparative study of the electronic structure of pure, Co-doped, and Ni-doped $BaFe_2As_2$. The $BaFe_2As_2$ doped by Co or Ni is considered at low concentration, in the orthorhombic phase when the compounds are SC with AFM order. The Co-doped $BaFe_2As_2$ was studied in our previous publication [41]. Here, we present the study of Ni-doped $BaFe_2As_2$, calculated at the same level of theory and compare with the results obtained for Co doping. The substitution of Fe by Co adds one electron to the system and the substitution of Fe by Ni adds 2 electrons. As we will discuss further, this produces not only quantitative but also qualitative effects. Even their phase diagrams are different.

The undoped $BaFe_2As_2$ exhibits a single structural/magnetic transition that splits into two distinct phase transitions (structural and magnetic transitions), both of which are suppressed when the Co concentration increases [39, 42, 43], see the phase diagram, Fig. 1. The SC phase appears when the Co concentration is greater than a critical concentration, at about $x \geq 0.033$ [42]. At this low Co concentration, the AFM phase and the SC phase coexist. However, at higher concentration, a magnetic transition

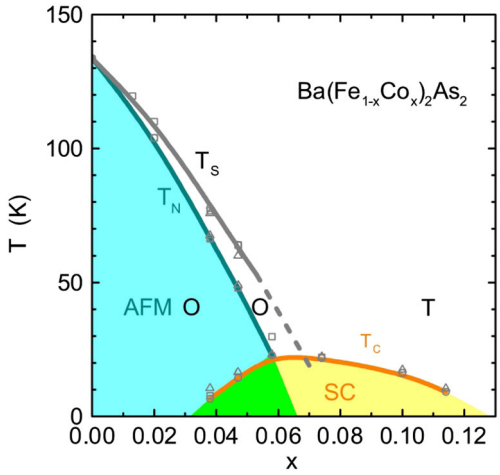


**Fig. 1** Phase diagram of $Ba(Fe_{1-x}Co_x)_2As_2$ superconductor as a function of Co concentration $x$, where $T$ paramagnetic tetragonal, $O$ paramagnetic orthorhombic, *AFM O* AFM ordered orthorhombic, and *SC* superconducting phases; $T_N$ magnetic (Néel) and $T_S$ structural phase transition temperatures (from ref. [39])

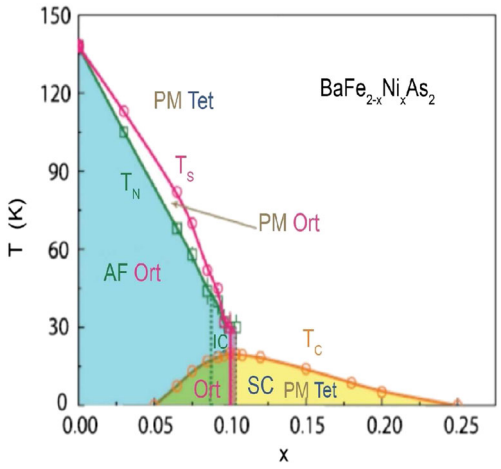


**Fig. 2** Electronic phase diagram of $BaFe_{2-x}Ni_xAs_2$ as a function of Ni concentration x, where *PM Tet* paramagnetic tetragonal, *PM Ort* paramagnetic orthorhombic, *AF Ort* commensurate AFM orthorhombic, *IC Ort* incommensurate AFM orthorhombic, and *SC* superconducting phases; $T_N$ magnetic (Néel) and $T_S$ structural phase transition temperatures (from ref. [48])

occurs and a nematic electronic liquid phase appears [44, 45], but the crystal is still SC with an orthorhombic structure [39, 43]. As was shown in ref. [46], using a microscopic model, the two transition lines—nematic and structural—penetrate separately in the superconducting dome. Deep in the superconducting dome up to $T = 0$ K, these two lines merge in a single first-order nematic-magnetic phase transition. Beyond $x = 0.06$, the tetragonal/orthorhombic transition as well as the nematic/paramagnetic transition are completed, and the SC critical temperature reaches its maximum (23 K) at the Co concentration $x \approx 0.07$ [42]. Another feature of the phase diagram is the coexistence of frozen antiferromagnetic domains and superconductivity for, $0.060 \leq x \leq 0.071$, as detected by $^{75}As$ nuclear magnetic resonance measurements [47]. At low temperature and for concentrations corresponding to the maximum $T_c$, spin glass clusters coexist with SC and a quantum critical point is also present [46].

The phase diagram for the Ni-doped material, $BaFe_{2-x}Ni_xAs_2$, was obtained from the study of structural and magnetic orders by high-resolution synchrotron x-ray and neutron scatterings [48] (Fig. 2). As we mention before, the parent compound exhibits a single structural/magnetic transition at 140 K that splits into two distinct phase transitions. However, these two transitions lines do not penetrate into the superconducting dome (contrary to the case of Co-doped $BaFe_2As_2$), but merge into a bicritical point 30 K, above its maximal transition temperature $T_c = 20.2$ K [48]. As was shown in ref. [49], at low temperature and concentration of Ni corresponding to the maximum $T_c$, the phase diagram for Ni-doping becomes similar to the phase diagram of Co-doping at the same conditions.

## 2 Methodology

The calculations were carried out using the electron-correlated embedded cluster method (ECM-MP2) developed by our group [50–52]. The ECM-MP2 methodology includes two stages. At the first one, the cluster that represents the material under study is selected and quantum mechanical calculations at the Møller-Plesset perturbation theory of the second-order level (MP2) are performed. The description of this perturbation theory, in which the Hartree-Fock approximation is used as a zero order, is presented in Appendix 3 of ref. [53]. At the second stage, a set of a finite number of point-like charges embedding the cluster and reproducing the Madelung potential of the infinite crystal on each atom of the cluster is arranged. This is achieved by adjusting the external charges of the charge array, see refs. [50, 51]. The determination of the cluster charge as well as the background charges depend on the material under study. Usually, charges taken from some crystal calculations or simple ionic model were used.

In this work for the representation of the ternary iron arsenide $BaFe_2As_2$, we select the cluster $Ba_4Fe_5As_8$ (Fig. 3). It is appropriate for study the modifications of the electronic structure upon substitution of the central Fe by Co or Ni atom because its symmetry properties correspond to a $D_2$ point group, a subgroup of the space group

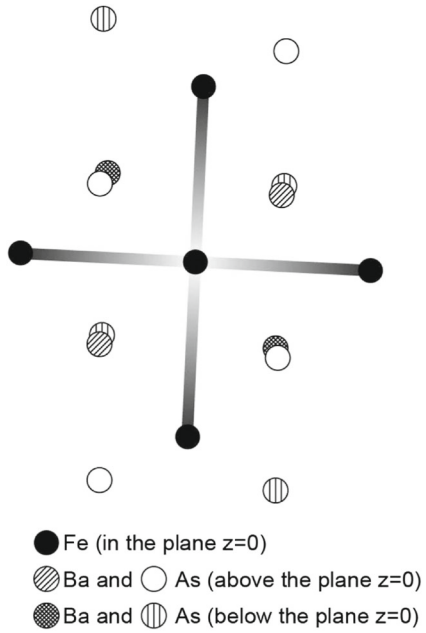


**Fig. 3** Cluster $Ba_4Fe_5As_8$

of $BaFe_2As_2$ crystal that belongs to the orthorhombic system. For the doped material, the clusters $Ba_4CoFe_4As_8$ and $Ba_4NiFe_4As_8$ were used, they are obtained by the substitution of the central Fe by the impurity atom. The number of atoms in our cluster, 17, is less than the unit cell atom number, 20. Therefore, our cluster is much smaller than the supercells used in ab initio calculations of bulk properties of pure or doped materials; the edge length of these supercells is generally equals to twice the lattice parameter (8 unit cells) [54–56]. Also, our methodology (ECM-MP2) is based on an electron correlated post-SCF method with localized electrons and provided by the Gaussian program; our methodology is quite different from that used in bulk property calculations generally based on DFT. Therefore, for these two reasons, our results cannot be applied to the study of bulk properties of materials.

The undoped material $BaFe_2As_2$ is a semimetal; in this case, the atomic charge can be taken as the Löwdin charges obtained from a calculation of the electronic structure at the DFT level using the QUANTUM ESPRESSO package [57]. The plane-wave DFT calculations [58] were performed at the local spin density approximation (LSDA), with the Perdew-Burke-Ernzerhof exchange-correlation potential; for more details, see our previous publication [41]. The structural information on the system under investigation (in this case, a unit cell) is taken from ref. [4].

The charges obtained from the DFT calculation are not consistent with a neutral unit cell and with the fact that we require an odd integer cluster charge to simulate a magnetic structure in our calculation of the pure $BaFe_2As_2$ represented by the cluster $Ba_4Fe_5As_8$. Therefore, the charges on the cluster atoms were readjusted to give a cluster charge $q = -1$. Then, the background charges are obtained through iterative procedure [50, 51] in order to reach self-consistency between background charges and cluster charges obtained from quantum calculations maintaining the cluster charge $q = -1$. In our case, the final background charges are 0.0138, 0.333, and −0.3402 for Ba, Fe, and As, respectively.

The quantum calculations of the cluster with its background charges were performed with the Gaussian-09 program [59]. For Fe and As atoms, all electrons were taken into account with the standard triply split valence basis set 6-311G(d); for Ba atoms, the Wood-Boring [59] pseudopotential was used. The calculations were performed by unrestricted in spin approach. Therefore, for obtaining a proper value of spin, the Gaussian spin projection procedure was used. The charges on atoms and the orbital populations were found by the natural bond orbital (NBO) analysis.

## 3 Results

In non-relativistic calculations, the Hamiltonian does not depend on the spin, the operator of the square of the spin angular momentum $\mathbf{S}^2$ commutes with the Hamiltonian, and spin $S$ is a good quantum number. That means that the energy levels of calculated clusters are classified according to the values of the total cluster spin S, or the multiplicity $M = 2S + 1$. In Table 1, we report the electronic cluster energy for different multiplicities. In this table, the corresponding eigenvalues of the operator $\mathbf{S}^2$ given by the

**Table 1** Cluster energy obtained by ECM-MP2 method

| Multiplicity | Energy (au) | $\mathbf{S}^2$ ($\hbar^2$) |
|---|---|---|
| (a) $Ba_4Fe_5As_8$ | | |
| 2 | −24293.26215 | 2.10 (1.97) |
| 4 | −24293.25282 | 3.87 (3.75) |
| 6 | −24293.26702 | 8.98 (8.76) |
| 8 | −24293.21967 | 15.92 (15.76) |
| (b) $Ba_4CoFe_4As_8$ | | |
| 1 | −24412.3754643 | 0.0 |
| 3 | −24412.2964173 | 3.31 (2.71) |
| 5 | −24412.2963723 | 6.13 (6.00) |
| 7 | −24412.2872351 | 12.19 (12.00) |
| (c) $Ba_4NiFe_4As_8$ | | |
| 2 | −24538.69836 | 2.18 (2.56) |
| 4 | −24538.78151 | 3.87 (3.75) |
| 6 | −24538.68251 | 9.16 (8.77) |
| 8 | −24538.63233 | 16.16 (15.76) |

equation $S(S + 1)$ and the corrected on the spin contamination values (in parenthesis) are also presented. The cluster energy is obtained by subtraction the self-energy of the background charges from the energy of the charge array constituted by the cluster charges plus the point-like background charges; both energies are given in the output of the Gaussian program.

As follows from Table 1, the ground state energy of $Ba_4Fe_5As_8$ cluster (it represents the undoped, or pure, $BaFe_2As_2$) is obtained for $S = 5/2$ ($M = 6$). For all values of spin, except $S = 1/2$ ($M = 2$), the correction on the spin contamination is very precise, whereas for $S = 1/2$ instead of $S(S + 1) = 0.75$, the value 1.97, corresponding to $S = 1$, is obtained. Thus, the result for $S = 1/2$ must not be taken into account.

In Ni-doped cluster, the ground state evidently corresponds $S = 3/2$ ($M = 4$); the state with $S = 1/2$ ($M = 2$), as in the case of the pure material, must not be taken into account. In Co-doped cluster, the ground state corresponds to $S = 0$. It is non-magnetic state and we will not consider it here, see discussion in ref. [41]. On the other hand, the states with $S \neq 0$, namely with $S = 1$ and $S = 2$ are degenerated. In both cases, we have an orthorhombic phase at low temperature when magnetic order and superconductivity coexist.

From Table 1, the difference between the energy of the doped cluster and that of the pure cluster can be extracted. This energy difference is a part of the impurity enthalpy of formation [54–56] but it has no sense to present it in this paper, since our calculations do not concern bulk properties.

To facilitate comparisons with the pure material later on, in Tables 2 and 3, we report also the charge distribution and the spin distribution in the parent compound. Here, we mention only that our results for the parent compound agree with two properties of the pure material: (1) a ferromagnetic alignment along the b axis and (2) the existence of so-called orbital order [60, 61] that results from a less occupation of $3d_{xz}$ and $3d_{yz}$ orbitals on a axis than the occupation of these orbitals on the b axis. Our results reinforced the assumption that the orbital order is responsible for anisotropies observed in different experiments [62–64].

The charge on atoms and the valence orbital population obtained by the NBO analysis at the MP2 level for pure, Co-doped, and Ni-doped $BaFe_2As_2$ are presented in Table 2. The results show an overall symmetry consistent with the $D_2$ point group. On the other hand, the results relative to the external As and Ba atoms of the cluster, which are in an environment of symmetry different from $D_2$, are not reported. The small populated excited orbitals corresponding to the Rydberg states as well as the population of Fe(4p) atoms, which are always small, are also not reported, but their population is taken into account in the final values of atomic charges (second column in Table 2).

When we look at the atomic charges, we observe a small increase of the positive charge on Fe-a for Co or Ni

**Table 2** Charge distribution at the MP2 level in pure and doped $Ba_4Fe_5As_8$ cluster (NBO analysis)

| | Atomic charge | Valence orbital population | Detailed charge and spin population on 3d(Fe) and 4p(As) orbitals |
|---|---|---|---|
| (a) $Ba_4Fe_5As_8$ ($S = 5/2$) | | | |
| Fe | 0.82 | $4s^{0.46}3d^{6.61}$ | $d_{xy}^{1.91} + d_{xz}^{1.95} + d_{yz}^{1.87} + d_{x^2-y^2}^{0.39} + d_{z^2}^{0.48}$ |
| Fe(n.n.)-a | 0.76 | $4s^{0.49}3d^{6.65}$ | $d_{xy}^{1.72} + d_{xz}^{0.68} + d_{yz}^{0.67} + d_{x^2-y^2}^{1.67} + d_{z^2}^{1.91}$ |
| Fe(n.n.)-b | 0.51 | $4s^{0.91}3d^{6.48}$ | $d_{xy}^{0.89} + d_{xz}^{1.49} + d_{yz}^{1.02} + d_{x^2-y^2}^{1.61} + d_{z^2}^{1.47}$ |
| As(n.n.) | −1.13 | $4s^{1.74}4p^{4.34}$ | $p_x^{1.41} + p_y^{1.56} + p_z^{1.37}$ |
| As(n.n.) | −1.13 | $4s^{1.74}4p^{4.34}$ | $p_x^{1.41} + p_y^{1.56} + p_z^{1.37}$ |
| (b) $Ba_4CoFe_4As_8$ ($S = 1$) | | | |
| Co | 1.03 | $4s^{0.48}3d^{7.35}$ | $d_{xy}^{1.94} + d_{xz}^{1.95} + d_{yz}^{1.96} + d_{x^2-y^2}^{0.33} + d_{z^2}^{1.18}$ |
| Fe(n.n.)-a | 0.80 | $4s^{0.47}3d^{6.62}$ | $d_{xy}^{1.92} + d_{xz}^{0.43} + d_{yz}^{0.82} + d_{x^2-y^2}^{1.56} + d_{z^2}^{1.89}$ |
| Fe(n.n.)-b | 0.49 | $4s^{0.93}3d^{6.48}$ | $d_{xy}^{1.03} + d_{xz}^{1.56} + d_{yz}^{0.96} + d_{x^2-y^2}^{1.41} + d_{z^2}^{1.53}$ |
| As(n.n.) | −1.35 | $4s^{1.74}4p^{4.74}$ | $p_x^{1.51} + p_y^{1.56} + p_z^{1.49}$ |
| As(n.n.) | −1.35 | $4s^{1.74}4p^{4.74}$ | $p_x^{1.51} + p_y^{1.56} + p_z^{1.49}$ |
| (c) $Ba_4NiFe_4As_8$ ($S = 3/2$) | | | |
| Ni | 0.91 | $4s^{0.47}3d^{8.43}$ | $d_{xy}^{1.73} + d_{xz}^{1.87} + d_{yz}^{1.07} + d_{x^2-y^2}^{1.92} + d_{z^2}^{1.84}$ |
| Fe(n.n.)-a | 0.84 | $4s^{0.47}3d^{6.57}$ | $d_{xy}^{1.89} + d_{xz}^{0.44} + d_{yz}^{0.80} + d_{x^2-y^2}^{1.59} + d_{z^2}^{1.86}$ |
| Fe(n.n.)-b | 0.49 | $4s^{0.94}3d^{6.47}$ | $d_{xy}^{1.42} + d_{xz}^{1.69} + d_{yz}^{0.85} + d_{x^2-y^2}^{1.05} + d_{z^2}^{1.46}$ |
| As(n.n.) | −1.30 | $4s^{1.74}4p^{4.40}$ | $p_x^{1.46} + p_y^{1.55} + p_z^{1.39}$ |
| As(n.n.) | −1.30 | $4s^{1.74}4p^{4.40}$ | $p_x^{1.46} + p_y^{1.55} + p_z^{1.39}$ |

**Table 3** Spin distribution at the MP2 level in pure and doped $Ba_4Fe_5As_8$ cluster (NBO analysis)

| | Atomic spin | Valence orbital spin population | Detailed spin population ($\alpha$ - $\beta$) on 3d(Fe) and 4p(As) orbitals |
|---|---|---|---|
| (a) $Ba_4Fe_5As_8$ ($S$ = 5/2) | | | |
| Fe | 0.31 | $4s^{0.01}3d^{0.30}$ | $d_{xy}^{-0.02} + d_{xz}^{0.00} + d_{yz}^{0.08} + d_{x^2-y^2}^{-0.02} + d_{z^2}^{0.27}$ |
| Fe(n.n.)-a | 0.08 | $4s^{0.00}3d^{0.08}$ | $d_{xy}^{0.00} + d_{xz}^{0.02} + d_{yz}^{0.11} + d_{x^2-y^2}^{-0.09} + d_{z^2}^{0.04}$ |
| Fe(n.n.)-b | 0.41 | $4s^{0.23}3d^{0.18}$ | $d_{xy}^{0.10} + d_{xz}^{-0.10} + d_{yz}^{0.25} + d_{x^2-y^2}^{-0.05} + d_{z^2}^{-0.02}$ |
| As(n.n.) | 0.11 | $4s^{0.02}4p^{0.09}$ | $p_x^{0.08} + p_y^{-0.03} + p_z^{0.04}$ |
| As(n.n.) | 0.11 | $4s^{0.02}4p^{0.09}$ | $p_x^{0.08} + p_y^{-0.03} + p_z^{0.04}$ |
| (b) $Ba_4CoFe_4As_8$ ($S$ = 1) | | | |
| Co | 0.98 | $4s^{0.01}3d^{0.96}$ | $d_{xy}^{0.02} + d_{xz}^{0.00} + d_{yz}^{0.00} + d_{x^2-y^2}^{0.01} + d_{z^2}^{0.93}$ |
| Fe(n.n.)-a | 0.01 | $4s^{0.00}3d^{0.02}$ | $d_{xy}^{0.03} + d_{xz}^{-0.01} + d_{yz}^{-0.01} + d_{x^2-y^2}^{0.01} + d_{z^2}^{0.00}$ |
| Fe(n.n.)-b | −0.28 | $4s^{-0.21}3d^{-0.06}$ | $d_{xy}^{-0.11} + d_{xz}^{-0.06} + d_{yz}^{0.03} + d_{x^2-y^2}^{0.00} + d_{z^2}^{0.08}$ |
| As(n.n.) | −0.02 | $4s^{-0.02}4p^{0.00}$ | $p_x^{0.02} + p_y^{-0.01} + p_z^{-0.01}$ |
| As(n.n.) | −0.02 | $4s^{-0.02}4p^{0.00}$ | $p_x^{0.02} + p_y^{-0.01} + p_z^{-0.01}$ |
| (c) $Ba_4NiFe_4As_8$ ($S$ = 3/2) | | | |
| Ni | 1.04 | $4s^{0.02}3d^{1.02}$ | $d_{xy}^{0.06} + d_{xz}^{0.03} + d_{yz}^{0.87} + d_{x^2-y^2}^{0.02} + d_{z^2}^{0.04}$ |
| Fe(n.n.)-a | 0.02 | $4s^{0.00}3d^{0.02}$ | $d_{xy}^{-0.01} + d_{xz}^{0.02} + d_{yz}^{0.01} + d_{x^2-y^2}^{0.00} + d_{z^2}^{0.00}$ |
| Fe(n.n.)-b | 0.25 | $4s^{0.22}3d^{0.03}$ | $d_{xy}^{-0.01} + d_{xz}^{0.09} + d_{yz}^{-0.06} + d_{x^2-y^2}^{0.04} + d_{z^2}^{-0.03}$ |
| As(n.n.) | 0.00 | $4s^{0.00}4p^{0.00}$ | $p_x^{0.02} + p_y^{0.00} + p_z^{-0.02}$ |
| As(n.n.) | 0.00 | $4s^{0.00}4p^{0.00}$ | $p_x^{0.02} + p_y^{0.00} + p_z^{-0.02}$ |

doping and an increase of the negative charge of As ions in both cases of doping. Therefore, there is a negative charge transfer from Fe-a ions to As ions. However, the central impurity contributes also to this charge transfer. It is instructive to perform a detailed comparative analysis of orbital populations.

Let us begin from the pure crystal comparing its orbital population with the valence orbital population of free atoms; Fe: $4s^2\ 3d^6$, As: $4s^2\ 4p^3$. The valence orbital population of atoms in the pure crystal (represented by the $Ba_4Fe_5As_8$ cluster) shows a large decrease of the 4s orbital population on Fe (1.54e for central Fe, 1.51e for Fe-a, 1.09e for Fe-b) and an excess of 3d orbital population on Fe (0.61e for the central Fe, 0.65e for Fe-a, and 0.48e for Fe-b). The decrease of 4s orbital on As is small, only 0.26e, while all excess of negative charge of As is located on 4p orbital, 1.34e.

In the doped crystal, the 3d population excess on central atom (dopand) decreases from 0.61e in the pure crystal to 0.35e in the case of Co doping and to 0.47e for Ni doping. Thus, there is also a contribution of the central impurities to the charge transfer from cations to anions. In the doped material, we have a charge transfer from impurities and Fe-a ions to 4p(As) orbitals. We observe that upon doping the $3d_{z^2}$(Co) orbital and the $3d_{yz}$(Ni) orbital are occupied approximately by one electron, while the other 3d(Co) and 3d(Ni) orbitals are almost completely filled; thus, the spin on Co and Ni must be near $S$ = 1/2. The occupation of some of 3d(Fe) orbitals are also near to unity; in the case of Co-doping, these are the $3d_{yz}$(Fe-a) and $3d_{yz}$(Fe-b) orbitals, whereas for Ni-doping, these are the $3d_{yz}$(Fe-a), $3d_{yz}$(Fe-b), and $3d_{x^2-y^2}$(Fe-b) orbitals.

The results for the spin distribution are presented in Table 3. Let us analyze the modifications of the spin distribution when the pure $BaFe_2As_2$ is doped with Co or Ni impurities. We note a large increase of the spin density on the central atom of doped clusters; the spin density on the Co or Ni atom is now three times greater than the spin density on the central Fe atom in the undoped cluster, while the spin densities on Fe and As atoms decrease. The overall modification of the spin distribution is characterized by a spin density transfer from Fe and As atoms to the central impurity; it corresponds to the transfer from 4p(As) and 3d(Fe) orbitals to $3d_{z^2}$(Co) and $3d_{yz}$(Ni) orbitals. Thus, the spin transfer occurs in opposite direction in comparison with charge transfer. This result reflects the independency of the spin and charge systems in the non-relativistic systems.

The spin density on orbitals $3d_{z^2}$(Co) and $3d_{yz}$(Ni) corresponds to almost one electron; these results are consistent with that observed for the charge density. Since the spin population on the others 3d orbitals and on 4s orbitals of the Co and Ni atoms is practically zero, the atoms-dopants have $S$ = 1/2. For Ni, this result is an agreement with the experimental measurements [40]. It should be also mentioned that for Co doping and for Ni doping as well, the spin density on Fe-a is decreasing to zero. A decrease of the magnetic moment on Fe as Co concentration increases is reported in

several experiments [39, 43, 44]; so our results are in a qualitative agreement with experimental observations. It is also important to mention that according to Tables 2 and 3, the orbitals $3d_{yz}$(Fe-a) and $3d_{yz}$(Fe-b) for Co doping and the orbitals $3d_{yz}$(Fe-a), $3d_{yz}$(Fe-b), and $3d_{x^2-y^2}$(Fe-b) for Ni doping are occupied practically by single electron with zero spin density. These spinless electrons resemble the spinless holons in the Anderson RVB model of high $T_c$ superconductivity [27–29], see discussion in our previous publication [41].

In spite of many similar properties of the Co- and Ni-doped $BaFe_2As_2$ crystal, their local magnetic properties are different. But before discussing it, we would like to mention that the size of the cluster we consider is not sufficient to reproduce all properties of the studied material. In particular, magnetic order along the **c** axis cannot be reproduced since we have only one iron plane. However, the magnetic order along the **b** axis can be obtained. On the other hand, an increase of our cluster size will add atoms at a distance from the impurity greater than that of the nearest neighbors and their influence will be smaller. Therefore, it should not lead to qualitative changes of the obtained results.

In the Co case, we note a sign reversal of the spin density on Fe-b ions: instead of 0.23 in the cluster representing the pure material, in doped cluster it is −0.21. This induces a local AFM order along the **b** axis; 4s(Fe-b) electrons and 3d electrons on (Fe-b) and on Co are responsible for the AFM order. The formation mechanism of the magnetic moment corresponds to a frustrated spin 1/2 $J_1$ - $J_2$ AFM Heisenberg model. According to discussion in ref. [26], this model is connected with Anderson's RVB theory of superconductivity.

In the Ni case, we observe a local ferromagnetic order along the b axis on the orbitals 4s(Fe-b), 3d(Fe-b) and 3d(Ni).

## 4 Conclusions

The results of our theoretical study are based on the ECM-MP2 computational methodology applied to $BaFe_2As_2$ doped with Co or Ni impurities. Most of our calculation results are confirmed by experimental measurements. The obtained, for undoped material, different occupation of $3d_{xz}$ and $3d_{yz}$ orbitals on the a and b axes (the so-called orbital order) reinforces the assumption that the orbital order is responsible for anisotropies observed in many experiments.

In the doped crystal, the charge and spin transfer was revealed. For both Co and Ni doping, the spin transfer occurs in opposite direction in comparison with charge transfer. This result reflects the independency of the spin and charge systems in the non-relativistic systems. We observe also a spinless electron (cf. the Anderson holon) on, in practice, the same orbitals for Co and Ni doping. From this follows, as we discussed in Section 3, that a model of superconductivity based on the Anderson RVB theory can be a good option. In all cases, we note also a large contribution of 4s(Fe-b) electrons to the formation of magnetic moment on Fe-b.

In the Ni-doped material, the magnetic structure on the b axis is locally ferromagnetic, similar to that of the parent compound; while in the case of Co doping, the magnetic order is different: we obtained a local AFM order along the b axis. Despite the fact that the magnetic order in Ni-doped $BaFe_2As_2$ is different from that of Co-doped $BaFe_2As_2$, in both cases, we found a spinless electron; thus, its presence is independent of the magnetic state. Our results, which are consistent with experimental observations, are obtained by a methodology based on localized electrons. Therefore, it can be concluded that the properties of Fe-based superconductors can be described from the viewpoint of localized electrons and not only from that of itinerant electrons [65, 66].

**Acknowledgments** The authors thank the DGTIC computer staff for providing access to the MITZLI clusters of Universidad Nacional Autonoma of México.

## References

1. Kamihara, Y., Watanabe, T., Hirano, M., Hosono, H.: J. Am. Chem. Soc. **130**, 3296 (2008)
2. Takahashi, H., et al.: Nature (London) **453**, 376 (2008)
3. Stewart, R.G.: Rev. Mod. Phys. **83**, 1589 (2011)
4. Rotter, M., et al.: Phys. Rev. **B78**, 020503 (2008)
5. Huang, Q., et al.: Phys. Rev. Lett. **101**, 257003 (2008)
6. Su, Y., et al.: Phys. Rev. **B79**, 064504 (2009)
7. Leithe-Jasper, A., Schnelle, W., Geibel, C., Rosner, H.: Phys. Rev. Lett. **101**, 207004 (2008)
8. Sefat, A.S., et al.: Phys. Rev. Lett. **101**, 117004 (2008)
9. Nishikubo, Y., et al.: J. Phys. Soc. Jpn. **79**, 095002 (2010)
10. Sefat, A.S., et al.: Phys. Rev. **B79**, 224524 (2009)
11. Sefat, A.S., et al.: Phys. Rev. **B85**, 024503 (2012)
12. Texier, Y., et al.: Eur. Phys. Lett. **99**, 17002 (2012)
13. Canfield, P.C. et al.: Phys. Rev. **B80**, 060501 (2009)
14. Mun, E.D., et al.: Phys. Rev. **B80**, 054517 (2009)
15. Laplace, Y., et al.: Phys. Rev. **B86**, 020510 (2012)
16. Singh, D.J., Du, M.H.: Phys. Rev. Lett. **100**, 237003 (2008)
17. Mazin, I.I., Singh, D.J., Johannes, M.D., Du, M.H.: Phys. Rev. Lett. **101**, 057003 (2008)
18. Mazin, I.I., Schmalian, J.: Physica **C469**, 614 (2009)
19. Wang, F., Lee, D.-H.: Science **332**, 200 (2011)
20. Norman, M.R.: Science **332**, 196 (2011)
21. Kuroki, K., et al.: Phys. Rev. Lett. **101**, 087004 (2008)
22. Kontani, H., Onari, S.: Phys. Rev. Lett. **104**, 157001 (2015)
23. Si, Q., Abrahams, E.: Phys. Rev. Lett. **101**, 076401 (2008)
24. Seo, K., Bernevig, B.A., Hu, J.P.: Phys. Rev. Lett. **101**, 206404 (2008)
25. Chen, W.-Q., Yang, K.-Y., Zhou, Y., Hang, F.-C.: Phys. Rev. Lett. **102**, 047006 (2009)

26. Lee, P.A., Nagaosa, N., Wen, X.-G.: Rev. Mod. Phys. **78**, 17 (2006)
27. Anderson, P.W.: Science **235**, 1196 (1987)
28. Kivelson, S.A., Rokhsar, D.S., Sethna, J.P.: Phys. Rev. **B35**, 8865 (1987)
29. Anderson, P.W., Baskaran, G., Zou, Z., Hsu, T.: Phys. Rev. Lett. **58**, 2790 (1987)
30. Anderson, P.W., Schrieffer, R.: Phys. Today **44**, 54 (1991)
31. Poilblanc, D., Corboz, P.h., Schuch, N., Cirac, J.I.: Phys. Rev. **B89**, 241106 (2014)
32. Gosvami, P., Yu, R., Si, Q., Abrahams, E.: Phys. Rev. **B84**, 155108 (2011)
33. Yao, D.X., Carlson, E.W.: Phys. Rev. **B78**, 052507 (2008)
34. Basov, D.N., et al.: Rev. Mod. Phys. **83**, 471 (2011)
35. Yin, Z.P., Haule, K., Kotliar, G.: Nat. Mater. **10**, 932 (2011)
36. Schafgans, A.A., et al.: Phys. Rev. Lett. **108**, 147002 (2012)
37. Georges, A., de' Medici, L., Mravlje, J.: Annu. Rev. Condens. Matter Phys. **4**, 137 (2013)
38. Aron, C., Kotliar, G.: Phys. Rev. **B91**(R), 041110 (2015)
39. Pratt, D.K., et al.: Phys. Rev. Lett. **103**, 087001 (2009)
40. Liu, M., et al.: Nat. Phys. **8**, 376 (2012)
41. Soullard, J., Perez-Enriquez, R., Kaplan, I.G.: Phys. Rev. **B91**, 184517 (2015)
42. Ni, N., et al.: Phys. Rev. **B78**, 214515 (2008)
43. Lester, C., et al.: Phys. Rev. **B79**, 144523 (2009)
44. Nandi, S., et al.: Phys. Rev. Lett. **104**, 057006 (2010)
45. Fernandes, R.M., Abrahams, E., Schmalian, J.: Phys. Rev. Lett. **107**, 217002 (2011)
46. Fernandes, R.M., Maiti, S., Wölfle, P., Chubukov, A.V.: Phys. Rev. Lett. **111**, 5700 (2013)
47. Dioguardi, A.P., et al.: Phys. Rev. Lett. **111**, 207201 (2013)
48. Lu, X., et al.: Phys. Rev. Lett. **110**, 257001 (2013)
49. Lu, X., et al.: Phys. Rev **B90**, 024509 (2014)
50. Kaplan, I.G., Soullard, J., Hernandez-Cobos, J., Pandey, R.: J. Phys.: Condens. Matter **11**, 1049 (1999)
51. Kaplan, I.G., Hernandez-Cobos, J., Soullard, J.: Quantum Systems in Chemistry and Physics, pp. 143–158. Kluwer Academic, Dordrecht (2000)
52. Kaplan, I.G., Soullard, J., Hernandez-Cobos, J.: Phys. Rev. **B65**, 214509 (2002)
53. Kaplan, I.G.: Intermolecular Interactions. Physical Picture, Computational Methods and Model Potentials, p. 367. John Wiley & Sons, Chichester (2006)
54. Huang, Y., et al.: Sci. Rep. **5**, 12750 (2015). doi:10.1038/srep12750
55. Hirayama, N., et al.: Jpn. J. Appl. Phys. **54**, 07 JC05 (2015)
56. Hong, J., et al.: Nat. Commun. **6**, 6293 (2015). doi:10.1038/ncomms7293
57. Giannozzi, P., et al.: J. Phys: Condens. Matter **21**, 395502 (2009)
58. Giannozzi, P. arXiv:0906.2569
59. Frisch, M.J., et al.: Gaussian 09 Revision C, vol. 01. Gaussian Inc., Pittsburgh (2009)
60. Chen, C.-C., et al.: Phys. Rev. **B82**(R), 100504 (2010)
61. Lv, W., Phillips, P.: Phys. Rev. **B84**, 174512 (2011)
62. Nakajima, M., et al.: Proc. Natl. Acad. Sci. (USA) **108**, 12238 (2011)
63. Ishida, S., et al.: Phys. Rev. Lett. **110**, 207001 (2013). J. Am. Chem. Soc. **135**, 3158 (2013)
64. Chu, J.-H., Kuo, H.-H., Analytis, J.G., Fisher, I.R.: Science **337**, 710 (2012)
65. Qureshi, N., et al.: Phys. Rev. **B86**(R), 060410 (2012)
66. Evtushinsky, D.V.: Phys. Rev. **B89**, 064514 (2014)